Comparison of cluster mass methods in the local universe

Krarup, Lea

Comparison of cluster mass methods in the local universe

THESIS

submitted in partial fulfillment of the
requirements for the degree of

MASTER OF SCIENCE
in
PHYSICS

Author :	Lea Krarup
Student ID :	2360345
Supervisor :	Dr. Matthieu Schaller
Second corrector :	Prof.dr. Joop Schaye

Leiden, The Netherlands, June 10, 2024

Comparison of cluster mass methods in the local universe

Lea Krarup

Leiden Institute of Physics, Leiden University
P.O. Box 9500, 2300 RA Leiden, The Netherlands

June 10, 2024

Abstract

Measuring the masses of galaxy clusters can contribute to accurately testing cosmological models. A few methods are available to estimate the masses of clusters, which, however, return vastly different mass estimates. The exact reasons for these discrepancies are not well understood. Here we show that these differences also occur in the mass measurement of clusters in the SIBELIUS-FLAMINGO simulation. The masses were estimated using three methods based on the dynamics of galaxies within a cluster, the X-ray luminosity and the Sunyaev-Zeldovich effect from gas in the cluster. Since the structures in the SIBELIUS simulation are reconstructed from the physical universe, the clusters' mass results can be compared directly with the true mass of the particles in the simulation and with observational mass estimates from other studies. While the dynamical method was the least accurate, using the Sunyaev-Zeldovich method on the SIBELIUS-FLAMINGO data was the most precise method in predicting the true mass of the simulation. Since Sunyaev-Zeldovich effect mass estimates tend to produce lower results than dynamical estimates; this means there are fewer supermassive clusters in the local cosmic environment which is consistent with predictions from ΛCDM.

Contents

Version of June 10, 2024– Created June 10, 2024 - 09:20

Chapter 1

Introduction

1.1 Background

Galaxy clusters, colossal cosmic structures composed of numerous galaxies gravitationally bound together, offer insights into the underlying dynamics and composition of the universe. Central to our understanding of these objects is the accurate determination of their masses, a parameter essential for testing the accuracy of cosmological models, including ΛCDM.

Four methods are commonly used to estimate cluster masses. The dynamical method involves extracting information about a cluster's gravitational potential from the velocity dispersion of the galaxies in the cluster. This method has its foundations in the virial theorem, which relates a systems kinetic and potential energy. The X-ray method relates the observable X-ray luminosity of a cluster to the thermodynamic properties of the hot dense gas emitting the X-ray photon. The thermodynamic properties are then used to extrapolate the total mass function of the cluster. The method based on the thermal Sunyaev-Zeldovich (SZ) effect stems from observations of the cosmic microwave background (CMB). CMB photons passing through the gas of the cluster experience inverse Compton scattering. The amount of scattering depends on the amount of gas that the photons pass through, so these kinds of CMB distortions can be fitted to the mass of the cluster. Finally, there is the method of weak lensing, which is not the focus of this thesis. Weak lensing relates the distortions in the images of background objects to the mass of the foreground galaxy cluster that functions as a gravitational lens.

While these methods are based on different observables, they should arrive at similar if not the same mass estimates if the underlying assumptions made for each method are correct. However, studies often arrive at

different masses for a given cluster. Comparing these mass results, a natural conclusion is that some underlying effects are not well understood and therefore not included in the estimation (Stopyra et al., 2021).

1.2 Overview of the research project

To address the discrepancies in mass measurement, we turn to the SIBELIUS-FLAMINGO simulation; a smoothed particle hydrodynamics simulation with initial conditions recreating the structures of the local observed universe. Measuring the masses in a simulation using the same techniques as observational studies allows us to compare them to the cluster's true mass, and test the validity of the mass estimation method.

The SIBELIUS project connects the structure of the Local Group with its cosmic environment (Sawala et al., 2022). These initial conditions have previously been used for a dark-matter-only simulation, called SIBELIUS-DARK (McAlpine et al., 2022). However, by adding the hydrodynamic components of the FLAMINGO project (Schaye et al., 2023), the data from the SIBELIUS-FLAMINGO simulation can be used to perform the mass measurement methods that rely on the gas in the cluster.

We applied the dynamical, X-ray, and SZ methods on the SIBELIUS-FLAMINGO data to estimate the masses of the following six clusters that exist both in the real universe, as well as in the simulation: Hercules A (Abell 2199), Perseus (Abell 426), Norma (Abell 3627), Coma (Abell 1656), Leo (Abell 1367), and the Virgo cluster. These clusters' locations can be seen in the dark matter and gas projections Figure 1.1.

The data used for this thesis comprised a $z = 0$ snapshot of particle data from a simulation run of SIBELIUS-FLAMINGO as well as a corresponding SOAP (Spherical Overdensity and Aperture Processor) catalogue with subhalo properties. The SOAP catalogue was used to identify the six clusters by comparing their simulation coordinates to their location in the SIBELIUS-DARK simulation (McAlpine et al., 2022).

The mass was estimated from four different observational directions for each cluster and each method. One of them was chosen so that it corresponds to the line of sight of an observer located at the position of the Milky Way, which inevitably is the perspective of all cosmic observations performed by human astronomers in the real world. The other three perspectives were picked to align with the three Cartesian axes of the simulation, such that these three mass estimations are as independent from each other as possible. This was done to investigate whether observational mass estimate results of a Milky Way observer were biased compared to

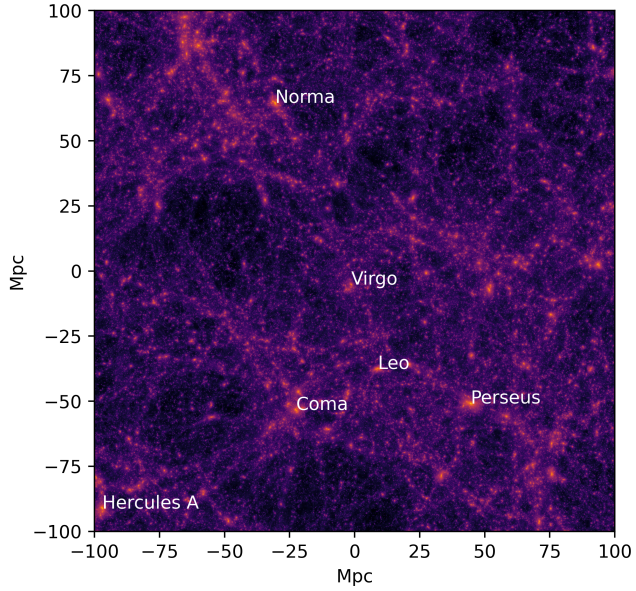

(a) Projection of the dark matter in the SIBELIUS-FLAMINGO snapshot.

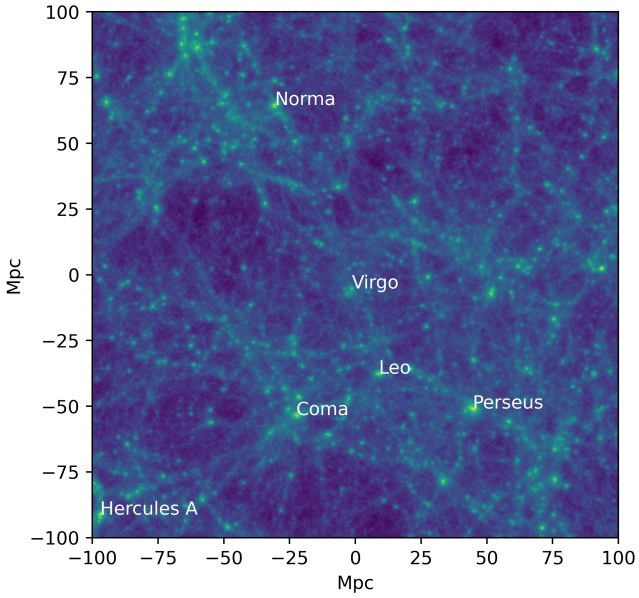

(b) Projection of the gas in the SIBELIUS-FLAMINGO snapshot.

Figure 1.1: Projections of the central 100 Mpc ***cube of the simulation.*** *The cube's center and origin of the coordinate system corresponds to the location of the Milky Way. The projection was performed using the SWIFTsimIO package (Borrow and Kelly, 2021).*

random perspectives.

Some of the methods assume that the cluster is spherical. To gauge qualitatively how valid that assumption is, a snapshot of each cluster was plotted using the same projection method as the dark matter in Figure 1.1a but with a smaller box size. The three most massive clusters can be seen in Figure 1.2, and the remaining three are depicted in Figure 1.3. Especially for the X-ray method, it is important to be aware that in reality, the clusters are not perfectly spherical objects, as assumptions such as symmetry and hydrostatic equilibrium are used in mass estimation. For some of the clusters, there are multiple density peaks at the centre, instead of one, which makes the cluster's shape oblong instead of spherical. An example of this is the Hercules A cluster in Figure 1.2a.

In the following three chapters, the dynamical, X-ray, and Sunyaev-Zeldovich methods will be introduced in more detail. For each of them, we will explain how they were implemented to work with the data from the SIBELIUS-FLAMINGO simulation. Each chapter ends with the simulation cluster mass estimate results obtained from using the method of that chapter. In the last chapter, the three methods are finally compared to each other and to the results from observational mass estimates.

1.3 The SIBELIUS-FLAMINGO simulation

The SIBELIUS project has created initial conditions for cosmological simulations resembling the structures in the real universe. This includes both the small-scale structures of the Local Group and the large-scale structures up to a comoving distance of 200 Mpc from the Milky Way.

The large-scale structures were found using the Bayesian Origin Reconstruction from Galaxies (BORG) algorithm (Jasche and Lavaux, 2019). The reconstruction is based on the 3D densities from 2M++ galaxy redshift catalogue. The BORG algorithm gives the most probable initial density field based on the survey, but only at scales larger than 3.91 Mpc. This leaves the small-scale structures at random. Sawala et al. (2022) kept the large-scale structures found with the BORG algorithm fixed and then randomised the small-scale structure in the central 16 cMpc box until structures with the properties of the Local Group formed. They ran 60000 simulations, and filtered through from criteria for the MW-M31 system, the nine most suitable simulations were selected. These nine candidates were further randomised on smaller scales to find systems with properties even closer to the Local Group.

For SIBELIUS-DARK, the simulation was run using 1.31×10^{11} dark

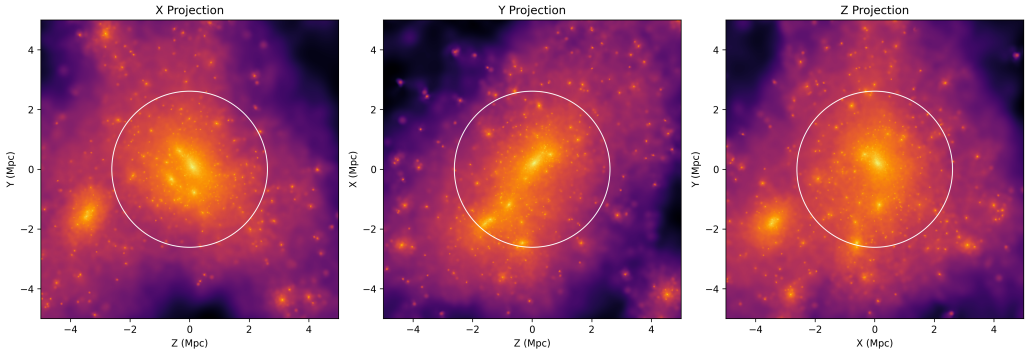

(a) Hercules A

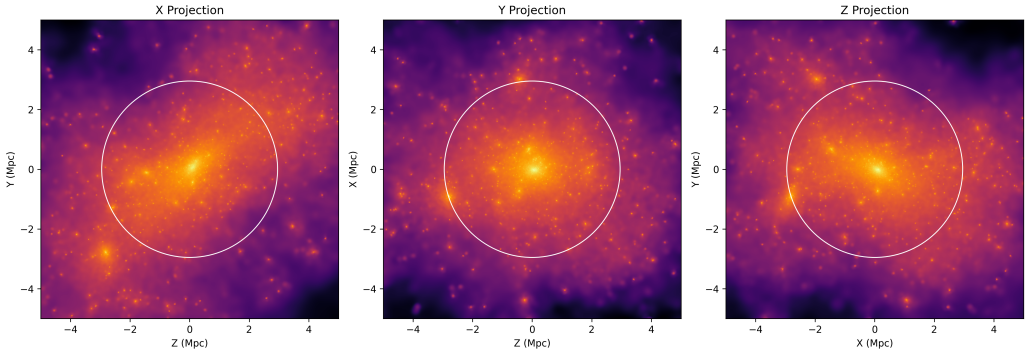

(b) Perseus

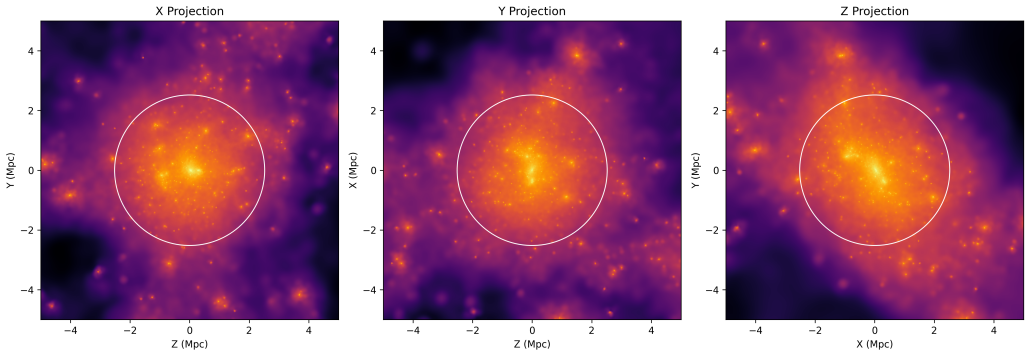

(c) Norma

Figure 1.2: The three most massive clusters projected along each simulation axis. *The dark matter particles are being projected using SWIFTsimIO (Borrow and Borrisov, 2020). The origin is located at the clusters centre of mass. The white circle indicates R_{200}, which approximately corresponds to the virial radius, the radius up to which the virial theorem applies (see Chapter 2).*

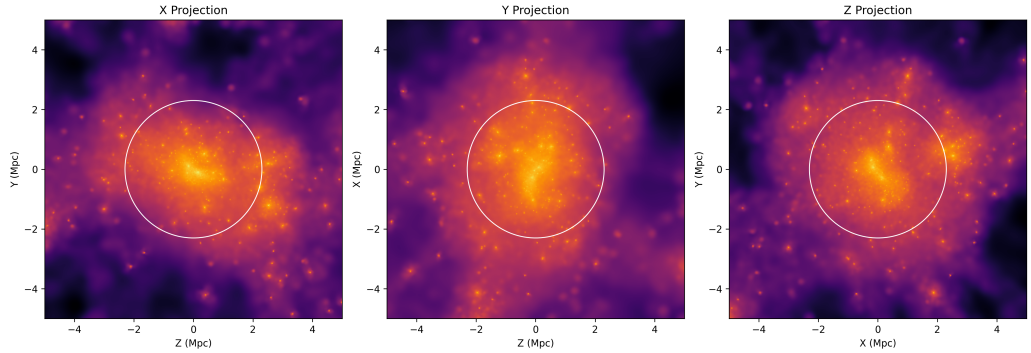

(a) Coma

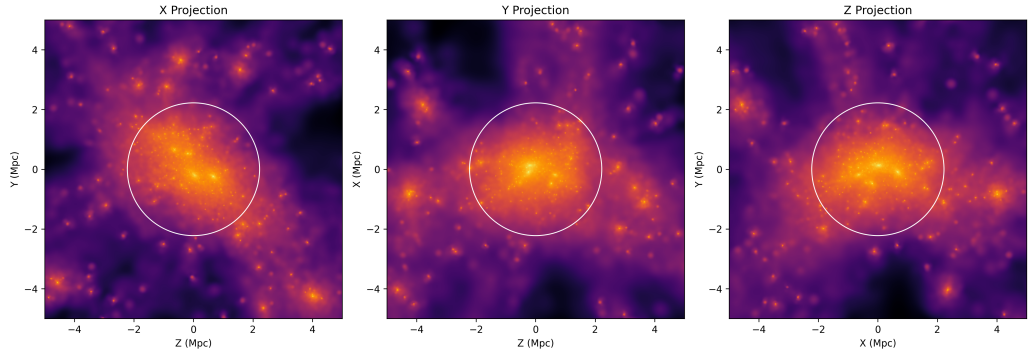

(b) Leo

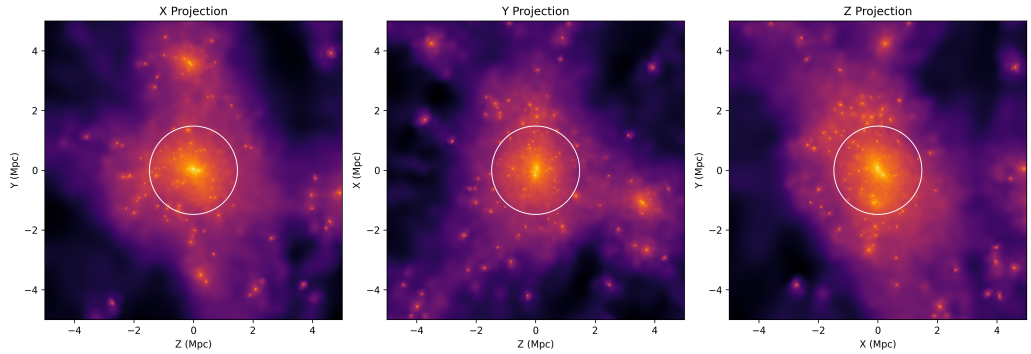

(c) Virgo

Figure 1.3: Three less massive clusters projected along each simulation axis. *As Figure 1.2, for the remaining 3 clusters.*

matter particles, less than 1×10^9 of which make up high-mass background particles. These background particles make up the region further than 200 Mpc away from the Local Group. This outer region is kept random, allowing for periodic boundary conditions. The dark matter particles in the constrained region have a mass of $1.15 \times 10^7\,\mathrm{M}_\odot$.

The SIBELIUS-FLAMINGO simulation used for this theses is made up of around 2.37×10^8 gas particles and 2.58×10^8 dark matter particles (including the background particles). The particle mass is $1.07 \times 10^9\,\mathrm{M}_\odot$ for the gas particles and $5.65 \times 10^9\,\mathrm{M}_\odot$ for the dark matter particles. This resolution is referred to as *intermediate* or *m9* by Schaye et al. (2023).

The simulation ran on the COSMA DiRAC facility at Durham University using the SWIFT cosmological simulation code Schaller et al. (2023). The halos were identified using the VELOCIraptor halo finder Elahi et al. (2019) and their halo properties were calculated using the Spherical Overdensity and Aperture Processor (SOAP) tool of the FLAMINGO project.

One of the halo properties in the catalogue is the total mass of each cluster. This property is key to this research, as it can be compared directly to the mass estimates from the dynamical, X-ray and Sunyaev-Zeldovich effect methods outlined in the next chapters. The total mass in the SIBELIUS-FLAMINGO simulation is made up of various types of matter compared to the dark-matter-only total mass present in the SIBELIUS-DARK simulation published in McAlpine et al. (2022). This difference in the simulation has little influence on the total mass of the clusters, as one can see in Table 1.1. Both the M_{200c} and M_{500c} masses in SIBELIUS-FLAMINGO are very close to the corresponding results from the SIBELIUS-DARK simulation published in McAlpine et al. (2022).

Cluster	DARK M_{200c}	DARK M_{500c}	FLAMINGO M_{200c}	FLAMINGO M_{500c}
Hercules A	$1.89 \times 10^{15}\,\mathrm{M}_\odot$	$1.13 \times 10^{15}\,\mathrm{M}_\odot$	$1.909 \times 10^{15}\,\mathrm{M}_\odot$	$1.196 \times 10^{15}\,\mathrm{M}_\odot$
Perseus	$2.72 \times 10^{15}\,\mathrm{M}_\odot$	$1.87 \times 10^{15}\,\mathrm{M}_\odot$	$2.749 \times 10^{15}\,\mathrm{M}_\odot$	$1.920 \times 10^{15}\,\mathrm{M}_\odot$
Norma	$1.72 \times 10^{15}\,\mathrm{M}_\odot$	$1.19 \times 10^{15}\,\mathrm{M}_\odot$	$1.709 \times 10^{15}\,\mathrm{M}_\odot$	$1.203 \times 10^{15}\,\mathrm{M}_\odot$
Coma	$1.27 \times 10^{15}\,\mathrm{M}_\odot$	$0.87 \times 10^{15}\,\mathrm{M}_\odot$	$1.297 \times 10^{15}\,\mathrm{M}_\odot$	$0.8972 \times 10^{15}\,\mathrm{M}_\odot$
Leo	$1.17 \times 10^{15}\,\mathrm{M}_\odot$	$0.84 \times 10^{15}\,\mathrm{M}_\odot$	$1.176 \times 10^{15}\,\mathrm{M}_\odot$	$0.8664 \times 10^{15}\,\mathrm{M}_\odot$
Virgo	$0.35 \times 10^{15}\,\mathrm{M}_\odot$	$0.27 \times 10^{15}\,\mathrm{M}_\odot$	$0.3452 \times 10^{15}\,\mathrm{M}_\odot$	$0.2570 \times 10^{15}\,\mathrm{M}_\odot$

Table 1.1: Simulation cluster masses. *The M_{200c} and M_{500c} masses of the SIBELIUS-DARK simulation (McAlpine et al., 2022) compared to the corresponding true simulation masses of the SIBELIUS-FLAMINGO run.*

Chapter 2

Dynamical method

2.1 Theory

Large astronomical objects are bound by the gravitational forces between their constituents. This can be characterised by the virial theorem. The virial system for an object with no external pressure, (e.g. a cluster) is (Mo et al., 2010):

$$2K + W = 0, \tag{2.1}$$

where W is the gravitational energy of the system and K is the system's kinetic energy. Since the total gravitational energy is dependent on the total mass of the system, the virial theorem can be used to estimate the mass of a cluster. This is done by treating the galaxies that are observed in the cluster as test particles (or tracers) and estimating their peculiar velocity and thus their kinetic energy through their redshift. One can thus define this mass as the *virial mass* M_{V}.

$$2\left\langle \frac{1}{2}mv^2 \right\rangle + \left\langle -\frac{GM_{\mathrm{V}}m}{r} \right\rangle = 0 \tag{2.2}$$

$$M_{\mathrm{V}} = \frac{\langle v^2 \rangle \langle r \rangle}{G} \tag{2.3}$$

To properly calculate this, one would need to know all three spatial components of the tracers as well as all three components in velocity space. As it is not possible to observe more than two spatial components and one velocity component of a distant astronomical object, we will use the following expression for the line of sight velocity dispersion $\sigma^2_{\mathrm{l.o.s.}}(R)$ from

(Schaller et al., 2015) to estimate the virial mass:

$$\sigma^2_{\text{l.o.s.}}(R) = \frac{2G}{\Sigma_*(R)} \int_R^\infty \frac{\mathcal{F}(r, R, \beta)\rho_*(r)M_{\text{tot}}(r)}{r^{2-2\beta}} \mathrm{d}r,, \tag{2.4}$$

where $\Sigma_*(R)$ is the observable 2D surface density of the tracer galaxies. As $\sigma^2_{\text{l.o.s.}}(R)$ and $\Sigma_*(R)$ are observables, and G is Newton's gravitational constant, only the expressions inside the integral need to be investigated further.

In the expression above, β is the velocity anisotropy parameter. Assuming isotropic velocity distribution,

$$\beta = 1 - \frac{\sigma^2_\theta}{\sigma^2_r} = 0, \tag{2.5}$$

the function $\mathcal{F}(r, R, \beta)$, can simply be expressed as (Schaller et al., 2015):

$$\lim_{\beta \to 0} \mathcal{F}(r, R, \beta) = \sqrt{r^2 - R^2} \tag{2.6}$$

The 3D density of galaxies $\rho_*(r)$ for simplicity's sake is approximated to be a $1/r^2$ function, normalised using the observable surface density $\Sigma_*(R)$.

The function $M_{\text{tot}}(r)$, the enclosed mass at radius r, can be split into the total mass within the cluster and the shape of the mass distribution. Defining the shape as $m(r)$, the dimensionless mass function ($\lim_{r\to\infty} m(r) = 1$), and the total mass of the cluster M_{V}, the function $M_{\text{tot}}(r)$ can be rewritten as

$$M_{\text{tot}}(r) = M_{\text{V}} m(r) \tag{2.7}$$

The mass is assumed to be distributed like a typical NFW dark matter halo (Mo et al., 2010).

$$\rho(r) = \rho_{\text{crit}} \frac{\delta_{\text{char}}}{(r/r_{\text{s}})\,(1 + r/r_{\text{s}})^2} \tag{2.8}$$

Instead of characterising the profile based on the scale radius r_{s}, the concentration parameter can be used. The parameter is related to the mass of the cluster (Comerford and Natarajan, 2007). A typical value for clusters $c = 4$ is used throughout this project.

$$c \equiv \frac{R_{\text{V}}}{r_{\text{s}}} \Rightarrow r_s = \frac{R_{\text{V}}}{c} \tag{2.9}$$

Integrating the density over a sphere of radius r, one can thus find an expression for $M_{\rm tot}(r)$ and for $M_{\rm V}$:

$$M_{\rm tot}(r) = 4\pi\rho_{\rm crit}\,\Omega_{\rm m}\delta_{\rm char}\,r_{\rm s}^3\left[\ln\left(1+c\frac{r}{R_{\rm V}}\right)-\frac{c\frac{r}{R_{\rm V}}}{1+c\frac{r}{R_{\rm V}}}\right] \tag{2.10}$$

$$M_{\rm tot}(R_{\rm V}) = M_{\rm V} = 4\pi\rho_{\rm crit}\,\Omega_{\rm m}\delta_{\rm char}\left(\frac{R_{\rm V}}{c}\right)^3\left[\ln(1+c)-\frac{c}{1+c}\right] \tag{2.11}$$

The dimensionless mass function $m(r)$ can then be constructed:

$$m(r) = \frac{M_{\rm tot}(r)}{M_{\rm V}} \tag{2.12}$$

$$m(r) = \frac{\ln\left(1+c\frac{r}{R_{\rm V}}\right)-\frac{c\frac{r}{R_{\rm V}}}{1+c\frac{r}{R_{\rm V}}}}{\ln(1+c)-\frac{c}{1+c}} \tag{2.13}$$

Therefore, equation (2.4) can be rewritten as

$$\sigma^2_{\rm l.o.s.}(R) = \frac{2GM_{\rm V}}{\Sigma_*(R)}\int_R^\infty \rho_*(r)\frac{\sqrt{r^2-R^2}}{r^2}\frac{\ln\left(1+c\frac{r}{R_{\rm V}}\right)-\frac{c\frac{r}{R_{\rm V}}}{1+c\frac{r}{R_{\rm V}}}}{\ln(1+c)-\frac{c}{1+c}}{\rm d}r. \tag{2.14}$$

Finally, solving for $M_{\rm V}$

$$M_{\rm V} = \frac{\sigma^2_{\rm l.o.s.}(R)\Sigma_*(R)}{2G\mathcal{I}(R)}, \tag{2.15}$$

with

$$\mathcal{I}(R) = \int_R^\infty \rho_*(r)\frac{\sqrt{r^2-R^2}}{r^2}\frac{\ln\left(1+c\frac{r}{R_{\rm V}}\right)-\frac{c\frac{r}{R_{\rm V}}}{1+c\frac{r}{R_{\rm V}}}}{\ln(1+c)-\frac{c}{1+c}}{\rm d}r, \tag{2.16}$$

one arrives at an expression for the virial mass using the observables available.

2.2 Methods

To utilise the virial theorem and Jeans equation as described above, one has to first identify which galaxies are in the cluster as they function as the tracers. Then one can use equations (2.15) and (2.16), to estimate the mass with the dynamical methods.

Version of June 10, 2024– Created June 10, 2024 - 09:20

2.2.1 Identifying galaxies

The dynamical method requires utilising the position of galaxies as well as their line of sight velocities to estimate the virial mass of the object. Therefore, the subhalos in the SOAP catalogue are required. While each subhalo has an associated parent halo as well as its three-dimensional position and velocity vectors listed in the catalogue, a Milky Way observer would only have the redshift of the galaxy as well as the two-dimensional position on the sky plane. This hypothetical observer therefore would have significantly less information to identify which galaxies are members of a given cluster than the information used in the catalogue to classify membership.

The position in the sky of the galaxy compared to the position of the cluster was determined as follows. The position vector of the subhalo was shifted to a coordinate system with its origin located at the centre of mass of the cluster. Then the position vector was projected onto the plane perpendicular to the observer's line of sight direction.

To emulate the redshift information available to an observer, the subhalos used in the dynamical estimate were picked using their line of sight peculiar velocity as well as cosmological redshift. For the distances within this project, Hubble's law can be used. The recessional velocity v_H of a galaxy at a distance d is then given by

$$v_H = H_0 d \tag{2.17}$$

where H_0 is the Hubble constant, the value $H_0 = 70\,\mathrm{km\,s^{-1}\,Mpc^{-1}}$ is used here. Then a galaxy is identified to be a part of the cluster if the sum of its line of sight peculiar velocity $v_{\mathrm{l.o.s.}}$ plus its recessional velocity v_H from the point of view of the observer is within a particular value of the sum of the bulk recessional velocity of the cluster and the clusters line of sight peculiar velocity.

All subhalos with the following three conditions were considered to be members of the cluster for the dynamical mass estimation method: The catalogue stellar mass of the subhalo being larger than $1 \times 10^{10}\,\mathrm{M_\odot}$, the sky radial distance to the cluster being less than the cluster's radius R_{500} in the catalogue, and the total line of sight velocity of the galaxy being within $1000\,\mathrm{km\,s^{-1}}$ of the redshift velocity of the cluster.

The number of subhalos identified in each cluster using this method was in the order of 100 galaxies per cluster. This quantity is significantly lower than the actual number of galaxies in a typical cluster because of the chosen minimum stellar mass requirement.

2.2.2 Estimating the dynamical mass

To estimate the masses of the clusters using the dynamical method, equation (2.15) was implemented in Python.

The surface density Σ was estimated by using the galaxies as tracers of the underlying density profile. Their radial positions were binned into 10 bins, and from that the surface density was calculated as the number of galaxies in a bin divided by the area of the annulus spanned by the bin edges. The velocity dispersion σ was calculated as the standard deviation of the line of sight velocities of the galaxies in the cluster. Finally, equation (2.16) was integrated numerically for the given radius.

It is important to note that, while R_{500} was used as the maximum radius of the subhalos selected and as input in any radius-dependent functions of equation (2.15), the resulting mass is the virial mass $M_V \approx M_{200}$, meaning the mass enclosed by the larger radius R_{200}.

2.3 Results

For each cluster, the mass was estimated as described above from four different directions. The first direction was from the perspective of a Milky Way observer looking towards the cluster. The other three directions were each parallel to one Cartesian simulation direction.

The results are depicted in Figure 2.1. The mass estimation results of each cluster are compared to the value of the cluster's mass in the catalogue. The catalogue value chosen is each cluster's M_{200}, as this is generally considered to be approximately equivalent to M_{V} (Mo et al., 2010). The grey line in the graph indicates where a mass estimate would lie if it were in perfect agreement with the catalogue value.

Hercules A The simulation catalogue lists the M_{200} mass of this cluster as $1.91 \times 10^{15}\,\mathrm{M}_\odot$. The Milky Way observer value is the closest of the dynamical mass estimation values at $2.89 \times 10^{15}\,\mathrm{M}_\odot$. The x-direction's value is an outlier at $11.2 \times 10^{15}\,\mathrm{M}_\odot$.

Perseus The results of the dynamical mass estimation for the Perseus cluster are close to each other ranging from $6.31 \times 10^{15}\,\mathrm{M}_\odot$ to $8.96 \times 10^{15}\,\mathrm{M}_\odot$ with the Milky Way value at $8.07 \times 10^{15}\,\mathrm{M}_\odot$. While being near each other, they are significantly higher than the catalogue value of $M_{200} = 2.75 \times 10^{15}\,\mathrm{M}_\odot$.

Norma The Milky Way result for the Norma cluster of $12.6 \times 10^{15}\,\mathrm{M}_\odot$. This is the value furthest from its corresponding catalogue value at

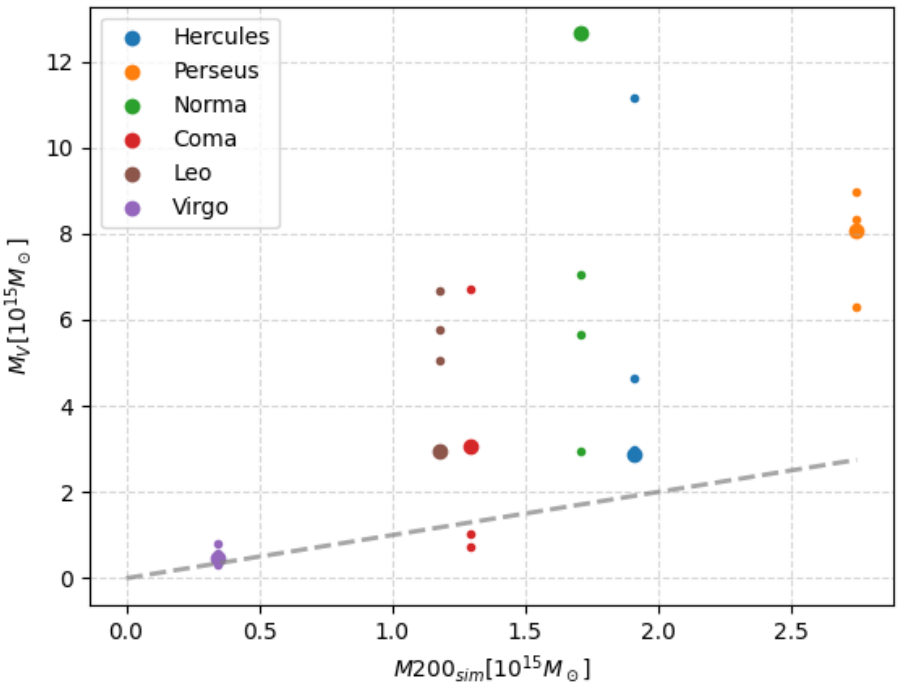

Figure 2.1: Dynamical method results. *The masses M_V found for the clusters compared to the catalogue M_{200} using the dynamical method. The larger circles indicate the measurement from the perspective of the Milky Way observer.*

$1.71 \times 10^{15}\,M_\odot$. The other perspectives have values in between those two, which range from $2.94 \times 10^{15}\,M_\odot$ to $7.04 \times 10^{15}\,M_\odot$.

Coma The dynamical mass results of the Coma cluster are spread around $M_{200} = 1.30 \times 10^{15}\,M_\odot$ with values from $0.732 \times 10^{15}\,M_\odot$ to $6.70 \times 10^{15}\,M_\odot$. The Milky Way value lies at $3.06 \times 10^{15}\,M_\odot$.

Leo The catalogue M_{200} of $1.18 \times 10^{15}\,M_\odot$ lies closest to the Milky Way result of $2.96 \times 10^{15}\,M_\odot$ while the other values range from $5.05 \times 10^{15}\,M_\odot$ to $6.68 \times 10^{15}\,M_\odot$.

Virgo All four points lie very close to the line. The results range from $0.313 \times 10^{15}\,M_\odot$ along the x-axis to $0.801 \times 10^{15}\,M_\odot$ along the y-axis. The Milky Way result is $0.479 \times 10^{15}\,M_\odot$. This value lies above the M_{200} value of $0.345 \times 10^{15}\,M_\odot$.

Looking at Figure 2.1, we find that the dynamical method as implemented

here is not very reliable. With the exception of the Virgo, most estimation values lie far away from the true simulation value. The Milky Way perspective value of the Norma cluster is the most extreme outlier. A probable reason for these outliers is a coincidental alignment of galaxies with the line of sight from the observer to the cluster. If the galaxy velocity lies within the expected value, this leads to a contamination of the mass measurement. These galaxies could be far away from the actual cluster due to the velocity being the sum of the peculiar and recessional velocity. This also explains why the method is more reliable for the Virgo cluster than for the other clusters: Since it has a very small recessional velocity compared to other clusters, there will be fewer galaxies that coincidentally have the right velocity to contaminate the measurement method.

Chapter 3

X-ray method

3.1 Theory

Assuming that the gas inside a cluster is in hydrostatic equilibrium, the gas pressure counteracts the gravitational forces experienced by the gas due to the mass of the cluster. Therefore, the gas in the centre of a gas-rich cluster is hot and dense plasma and thus emits bremsstrahlung in the form of X-ray photons. By observing the X-ray, astronomers can thus estimate the mass of a cluster by reconstructing the temperature and density profile of the gas.

For a gravitational potential in the cluster satisfying the Poisson equation (Mo et al., 2010)

$$\nabla^2\Phi(\mathbf{r}) = 4\pi G\rho(\mathbf{r}), \tag{3.1}$$

where $\rho(\mathbf{r})$ is the total matter density profile. The pressure gradient and the gravitational potential are related by

$$\nabla P(\mathbf{r}) = -\rho(\mathbf{r})\nabla\Phi(\mathbf{r}), \tag{3.2}$$

The radial component of the gravitational gradient can be found from equation (3.1):

$$\frac{\mathrm{d}\Phi}{\mathrm{d}r} = \frac{GM(r)}{r^2}, \tag{3.3}$$

and the radial component of the pressure gradient can be found from the ideal gas law ($P = nk_\mathrm{B}T$) with the number density expressed as $n = \rho/\mu m_\mathrm{u}$, where ρ is the mass density, μ the mean molecular mass of the gas, and m_u the atomic mass constant.

$$\frac{\mathrm{d}P}{\mathrm{d}r} = \frac{\mathrm{d}\left(k_\mathrm{B}T\rho/\mu m_\mathrm{u}\right)}{\mathrm{d}r} \tag{3.4}$$

Inserting (3.3) and (3.4) into equation (3.2), and solving for $M(r)$ (Mo et al., 2010),

$$M(r) = -\frac{k_B T(r) r}{\mu m_u G} \left[\frac{\mathrm{d} \ln \rho}{\mathrm{d} \ln r} + \frac{\mathrm{d} \ln T}{\mathrm{d} \ln r} \right], \tag{3.5}$$

we are left with an expression for the total mass of the cluster depending on a combination of the density and temperature. As the amount of X-ray emission of the cluster also depends on both the density and the temperature, the exact relation has to be calibrated using observations of many clusters and fitting the relation.

One study using this approach is Lovisari et al. (2020). To estimate the mass of the six clusters in this project, the model and fitted parameters from Lovisari et al. (2020) are used to determine the relation between the X-ray luminosity L_X and the total mass of the cluster M_{tot}:

$$\log\left(\frac{L_X}{C_1}\right) = \alpha + \beta \log\left(\frac{M_{tot}}{C_2}\right) + \gamma \log \frac{E(z)}{E(0.2)} \tag{3.6}$$

with $C_1 = 5 \times 10^{44}\,\mathrm{erg\,s^{-1}}$ and $C_2 = 6 \times 10^{14}\,\mathrm{M_\odot}$. The function $E(z)$ is dependent on the cosmological density parameters Ω

$$E(z) = \sqrt{\Omega_{\mathbf{m}}(1+z)^3 + \Omega_\Lambda} \tag{3.7}$$

with $\Omega_{\mathbf{m}} = 0.7$ and $\Omega_\Lambda = 0.3$. $\alpha = 0.089$, $\beta = 1.822$, and $\gamma = 0.462$ are the fitted parameters. For the snapshot used below, $z = 0$ for all particles. Solving equation (3.6) for the mass of the cluster

$$M_{tot} = C_2 \left(e^{-\alpha} \left(\frac{E(0.2)}{E(z)} \right)^{\gamma} \left(\frac{L_X}{C_1} \right) \right)^{1/\beta}, \tag{3.8}$$

we have an expression that can be used to estimate the mass of the cluster given a known X-ray luminosity of the cluster.

3.2 Methods

To estimate the cluster mass using X-ray luminosity, the gas particles in the cluster have to be identified and their X-ray luminosity added up. Once the X-ray luminosity of a cluster has been determined, equation (3.8) can be used to estimate the cluster's mass, specifically its M_{500}. However, since an astronomical observer's information about the position of the X-ray-emitting gas is limited to the 2D sky coordinates, the choice of which simulation particles are considered to be in the cluster is not trivial.

For each cluster, the particles in a cube much larger than the cluster (1% of the total simulation volume) were loaded using SWIFTsimIO (Borrow and Borrisov, 2020). To get an estimate of the observed radius of the cluster, the catalogue value R_{500} of the cluster was also loaded.

To identify which particles should be counted as being within the cluster, a cylindrical mask was used. This cylinder was centred around the centre of mass of the cluster in the SOAP catalogue. The radius of the cylinder was chosen to be R_{500}, while the height of the cylinder was chosen to be $10R_{500}$. The height of the cylinder was aligned along the line of sight of the observer. Therefore, hypothetical other close-by objects whose sky position aligned with the cluster could impact the results. Any particle within the cylinder was counted to be in the cluster.

In the SIBELIUS-FLAMINGO simulation, each gas particle has three different X-ray luminosity values corresponding to 3 different bandwidths. None of these bands match the bandwidth used in (Lovisari et al., 2020) ($0.1 - 2.4$ keV) for the fitted model (3.6) exactly. For this research, we used the simulation bandwidth *erosita_high* ($2.3 - 8.0$ keV).

The sum of the luminosity in that bandwidth of all the particles was converted from simulation units into physical units ($\mathrm{erg\,s^{-1}}$). This value was then used to determine the cluster mass by inserting it into (3.8).

3.3 Results

The X-ray masses of the six clusters were estimated from the same four different perspectives as for the dynamical method. One perspective was from an observer looking from the Milky Way, the other three were observers looking in a direction parallel to Cartesian axes.

The results of the X-ray mass estimation can be seen in Figure 3.1. Since it was the value of M_{500} that was estimated using the fitted model eq. (3.8), the estimates were plotted against the M_{500} value listed in the catalogue. All cluster mass results using the X-ray method were lower than their corresponding catalogue value.

Hercules A X-ray mass estimates for the Hercules A cluster range between $1.05 \times 10^{15}\,\mathrm{M}_\odot$ and $1.08 \times 10^{15}\,\mathrm{M}_\odot$, with the Milky Way observer's value at $1.06 \times 10^{15}\,\mathrm{M}_\odot$. The M_{500} in the catalogue is listed as $1.20 \times 10^{15}\,\mathrm{M}_\odot$.

Perseus The Perseus cluster's X-ray mass estimates range from $1.21 \times 10^{15}\,\mathrm{M}_\odot$ to $1.22 \times 10^{15}\,\mathrm{M}_\odot$. All estimates are lower than the catalogue value $M_{500} = 1.92 \times 10^{15}\,\mathrm{M}_\odot$.

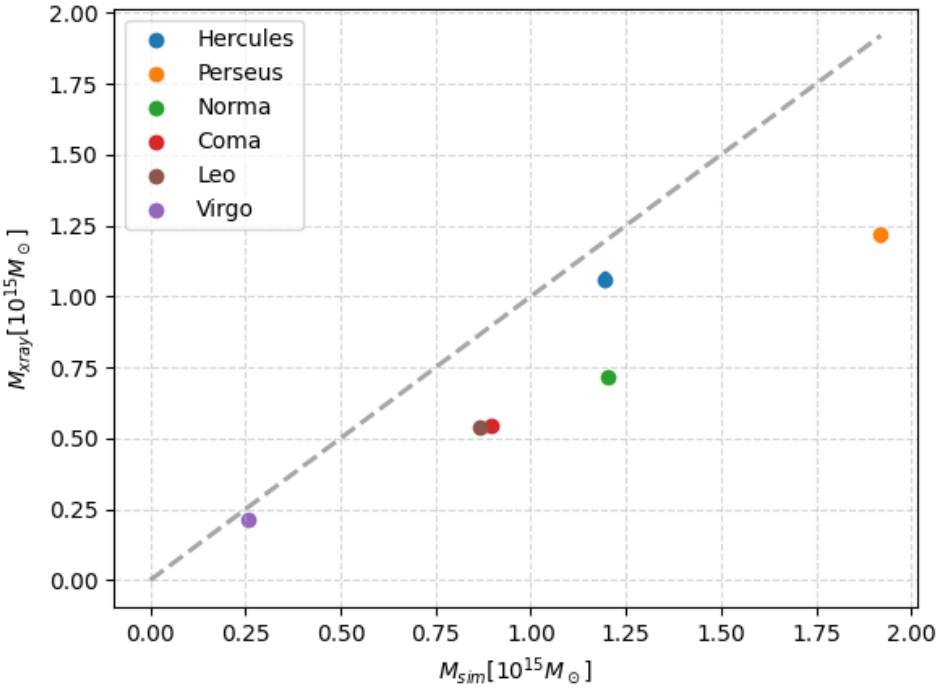

Figure 3.1: X-ray method results. *The masses M_{xray} found for the clusters compared to the catalogue M_{500} using the X-ray method. The larger circles indicate the measurement from the perspective of the Milky Way observer. Mostly hidden behind them are smaller circles with the perspective along the three Cartesian axes.*

Norma The Cartesian perspective X-ray mass estimates for the Norma cluster consistently measure around $0.717 \times 10^{15}\,\mathrm{M}_\odot$, and the Milky Way observer's value is $0.716 \times 10^{15}\,\mathrm{M}_\odot$. The estimates are therefore lower than its M_{500} catalogue value of $1.20 \times 10^{15}\,\mathrm{M}_\odot$.

Coma X-ray mass estimates for the Coma cluster vary between $0.544 \times 10^{15}\,\mathrm{M}_\odot$ and $0.551 \times 10^{15}\,\mathrm{M}_\odot$, with the Milky Way observer's value at $0.545 \times 10^{15}\,\mathrm{M}_\odot$, lower than its M_{500} catalogue value of $0.897 \times 10^{15}\,\mathrm{M}_\odot$.

Leo X-ray mass estimates for the Leo cluster are ranging from $0.537 \times 10^{15}\,\mathrm{M}_\odot$ to $0.540 \times 10^{15}\,\mathrm{M}_\odot$, with the Milky Way observer's value at $0.538 \times 10^{15}\,\mathrm{M}_\odot$. Its M_{500} catalogue value is $0.866 \times 10^{15}\,\mathrm{M}_\odot$.

Virgo The Virgo cluster's X-ray mass estimates consistently measure at

$0.212 \times 10^{15}\,\mathrm{M}_{\odot}$. This makes it lower than the M_{500} catalogue value of $0.257 \times 10^{15}\,\mathrm{M}_{\odot}$.

The perspective from which the method is used has little impact on the mass estimates. In Chapter 5, the Milky Way values will be used to compare them to observational X-ray results of the clusters' mass estimates from literature, as this perspective corresponds to the point of view of observations.

Notably, all six clusters' mass estimates lie below the corresponding catalogue value. One source of inaccuracy could be the model using a slightly different bandwidth than the FLAMINGO code. In addition to that, if the clusters are not in hydrostatic equilibrium at the time of the $z = 0$ snapshot, the mass estimates will not be accurate (Mo et al., 2010). In the case of the clusters still collapsing into their future structure, the temperature and density would not be large enough to counteract gravity yet and therefore the gas in the cluster would be emitting less gas. This in turn would mean that the mass estimate using this method on a collapsing cluster would be lower than its actual mass. Underestimating cluster masses due to assuming hydrostatic equilibrium is referred to as *hydrostatic mass bias* and is considered to be around 10-15% of the total mass (Planck Collaboration, 2014). Adding a bias term into the model used could thus improve the results of the X-ray mass estimation method.

Looking back at the images of the cluster shapes, Figures 1.2 and 1.3, and comparing them to the mass results in Figure 3.1, Hercules A sticks out as it both has a significant offset in its X-ray mass compared to the other clusters, and it has large substructures, and large nearby objects, which suggests that it most likely is far from hydrostatic equilibrium.

Chapter 4

Sunyaev-Zeldovich method

4.1 Theory

In the centre of clusters, there is dense and hot gas due to the gas pressure that has to counteract gravity. This phenomenon was discussed in chapter 3.1. When cosmic microwave background photons (CMB) reach this gas, the CMB photons interact with the gas via inverse Compton scattering, meaning that the photons gain energy from interacting with the free electrons in the plasma (Zeldovich and Sunyaev, 1969). This phenomenon is known as the Sunyaev-Zeldovich effect.

The Sunyaev-Zeldovich effect can be used to estimate the mass of a cluster. The temperature change in the CMB is linked to the electron pressure along the line of sight $P(\ell)$ in the gas through the following relation (Mo et al., 2010):

$$\frac{\delta T}{T} = -\frac{2\sigma_{\mathrm{T}}}{m_{\mathrm{e}}c^2}\int P_{\mathrm{e}}(\ell)\mathrm{d}\ell \tag{4.1}$$

where the Thomson cross-section $\sigma_T = 6.65 \times 10^{-25}\,\mathrm{cm}^2$. The electron pressure is dependent on both the temperature and density of the electrons and increased electron pressure thus corresponds to an increase in the distortion of the cosmic microwave background.

Since the density and temperature are also related to the X-ray emission and the mass of the cluster as discussed in the previous chapter, the results from X-ray surveys can be used to find the relation between the CMB distortions of a cluster Y_{500} and its mass M_{500}.

From the comparison of CMB distortions and X-ray surveys of many clusters, a model can thus be fitted to predict the mass. The Planck collab-

oration fitted the following relation (Planck Collaboration, 2014):

$$E^{-2/3}(z)\left[\frac{D_{\mathrm{A}}^2 Y_{500}}{10^{-4}\mathrm{Mpc}^2}\right] = 10^{-0.19\pm0.02}\left[\frac{(1-b)M_{500}}{6\times10^{14}M_{\odot}}\right]^{1.79\pm0.08}, \qquad (4.2)$$

with the bias parameter b fitted such that $(1-b) = 0.80$, and the function $E(z)$ given by equation (3.7). The bias parameter takes hydrostatic mass bias into account as X-ray masses assuming hydrostatic equilibrium and masses derived from X-ray underestimate the true mass. Solving this model for M_{500}, we are left with a cluster mass estimate using the Sunyaev-Zeldovich effect:

$$M_{500} = \left(10^{0.19}E^{-2/3}(z)\frac{D_{\mathrm{A}}^2 Y_{500}}{10^{-4}\mathrm{Mpc}^2}\right)^{\frac{1}{1.79}}\frac{6\times10^{14}\,\mathrm{M}_{\odot}}{(1-b)}. \qquad (4.3)$$

4.2 Methods

Overall, the process of estimating the cluster mass using the Sunyaev-Zeldovich effect was very similar to the method using X-ray emission. Each gas particle in the SIBELIUS-FLAMINGO simulation snapshot has the attribute *comptonY*, which indicates how much SZ effect the particle contributes to the cosmic microwave background. This means that one can sum up the *comptonY* for all the particles in the cluster, and use equation (4.3) to get an estimate for the M_{500} mass using the SZ effect.

The gas particles were loaded using SWIFTsimIO (Borrow and Borrisov, 2020) using a cubic mask much larger than the cluster. Then the particles' positions in the cluster's centre of mass frame were projected onto the observer's sky. The same cylinder as described in the previous chapter for the X-ray method was again used to determine the member gas particles of the cluster. The cylinder had radius R_{500}, height $10R_{500}$ and was aligned with the line of sight of the observer.

The *comptonY* attribute in the simulation, corresponds to $D_{\mathrm{A}}^2 Y_{500}$ in equation (4.3). While Y_{500} would be dependent on the distance to the cluster, each particle in the simulation has a *comptonY* value independent of where its observer is located. *comptonY* is therefore given in units of Mpc^2, which corresponds to the units of $D_{\mathrm{A}}^2 Y_{500}$ in equation (4.3).

To get an estimate for the cluster mass, the *comptonY* values of all the gas particles in the cylinder were added together. This sum was then inserted into equation (4.3) in the position of $D_{\mathrm{A}}^2 Y_{500}$. The result was an estimate of M_{500} using the thermal Sunyaev-Zeldovich effect.

4.3 Results

Using the SZ effect and equation (4.3) method described above, the mass M_{500} was estimated for the six clusters from the four different perspectives (Milky Way and Cartesian) used for the other methods.

These masses can be seen in Figure 4.1 compared to the M_{500} values in the catalogue. All results lie closely to the grey line, indicating a higher agreement with the catalogue than the other two methods had. It is, however, noteworthy that all results lie above the line, compared to the X-ray results (Figure 3.1) that were below the grey line.

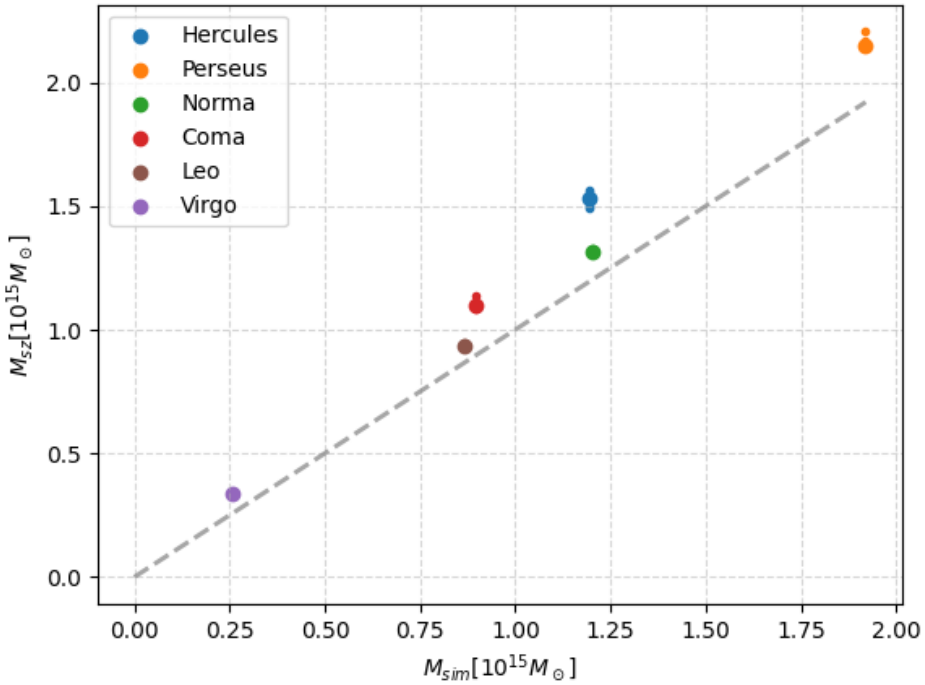

Figure 4.1: Sunyaev-Zeldovich effect results. *The masses M_{sz} found for the clusters using the SZ effect method compared to the catalogue mass M_{500}. The larger circles indicate the measurement from the perspective of the Milky Way observer. Hidden behind the larger circles are smaller ones with the perspectives along the three Cartesian axes.*

Hercules A SZ mass estimates for Hercules A cluster vary between $1.49 \times 10^{15}\,M_\odot$ and $1.56 \times 10^{15}\,M_\odot$, with the Milky Way observer's value

Version of June 10, 2024– Created June 10, 2024 - 09:20

at $1.53 \times 10^{15}\,\mathrm{M}_{\odot}$, notably higher than its M_{500} catalogue value of $1.20 \times 10^{15}\,\mathrm{M}_{\odot}$.

Perseus The Perseus cluster's SZ mass estimates range from $2.15 \times 10^{15}\,\mathrm{M}_{\odot}$ to $2.20 \times 10^{15}\,\mathrm{M}_{\odot}$, with the Milky Way observer's value being $2.15 \times 10^{15}\,\mathrm{M}_{\odot}$, and surpassing its M_{500} catalogue value of $1.92 \times 10^{15}\,\mathrm{M}_{\odot}$.

Norma SZ mass estimates for the Norma cluster range between $1.31 \times 10^{15}\,\mathrm{M}_{\odot}$ and $1.33 \times 10^{15}\,\mathrm{M}_{\odot}$, with the Milky Way observer's value at $1.32 \times 10^{15}\,\mathrm{M}_{\odot}$, all exceeding its M_{500} catalogue value of $1.20 \times 10^{15}\,\mathrm{M}_{\odot}$.

Coma For the Coma cluster, SZ mass estimates vary between $1.08 \times 10^{15}\,\mathrm{M}_{\odot}$ and $1.14 \times 10^{15}\,\mathrm{M}_{\odot}$, with the Milky Way observer's value at $1.10 \times 10^{15}\,\mathrm{M}_{\odot}$, higher than its M_{500} catalogue value of $0.897 \times 10^{15}\,\mathrm{M}_{\odot}$.

Leo SZ mass estimates for the Leo cluster range from $0.927 \times 10^{15}\,\mathrm{M}_{\odot}$ to $0.949 \times 10^{15}\,\mathrm{M}_{\odot}$, with the Milky Way observer's value at $0.934 \times 10^{15}\,\mathrm{M}_{\odot}$, all surpassing its M_{500} catalogue value of $0.866 \times 10^{15}\,\mathrm{M}_{\odot}$.

Virgo The Virgo cluster's SZ mass estimates are consistent a ranging from $0.331 \times 10^{15}\,\mathrm{M}_{\odot}$, to $0.335 \times 10^{15}\,\mathrm{M}_{\odot}$, the latter being Milky Way observer's value, and exceeding its M_{500} catalogue value of $0.257 \times 10^{15}\,\mathrm{M}_{\odot}$.

While the SZ effect method generally produced the closest results, there seems to be a slight systematic tendency to overestimate the mass of the cluster. One reason for this could be a small difference in the underlying model assumptions of the fitted model used here, and the model for the *comptonY* attribute in the FLAMINGO code. Despite the model being based on X-ray, this method performs better than the X-ray method. This is most likely due to the bias parameter used for the model in this chapter but not for the model in the X-ray chapter. This parameter compensates for an underestimation of the mass due to hydrostatic mass bias of the underlying X-ray model.

Chapter 5

Discussion and conclusion

5.1 Comparison of methods

After investigating each method individually, we examined how well the cluster mass measurement methods performed. Comparing Figures 2.1, 3.1, and 4.1 from the previous chapters, we can see that the three methods were not equally effective at predicting the clusters' true masses from the catalogue.

The clear winner among the three mass estimation methods was the Sunyaev-Zeldovich method. Its estimates for each cluster were very close to the simulation truth from the catalogue and significantly outperformed the other methods discussed in this study. The X-ray method was the second-most and the dynamical method was the least effective. One reason could be that the dynamical method is derived directly from theory. The model was simplified such that all the parameters were known. The X-ray and Sunyaev-Zeldovich results were based on more complex models that were fitted using many real observations of clusters.

At a glance, it may seem surprising, why the SZ method performs better as a mass estimation method than the X-ray method since the model equation (4.3) used for the Sunyaev-Zeldovich method was fitted using results from an X-ray survey (Planck Collaboration, 2014). The key to understanding this is hydrostatic mass bias. While the X-ray and Sunyaev-Zeldovich effect methods have assumptions about symmetry and the dynamics of the intra-cluster medium, our findings suggest that including a bias term can compensate for that sufficiently. This explains why the Sunyaev-Zeldovich effect estimates were more precise, as the model included a bias term to compensate for hydrostatic mass bias, while the X-ray estimate was done without including the bias as the X-ray model

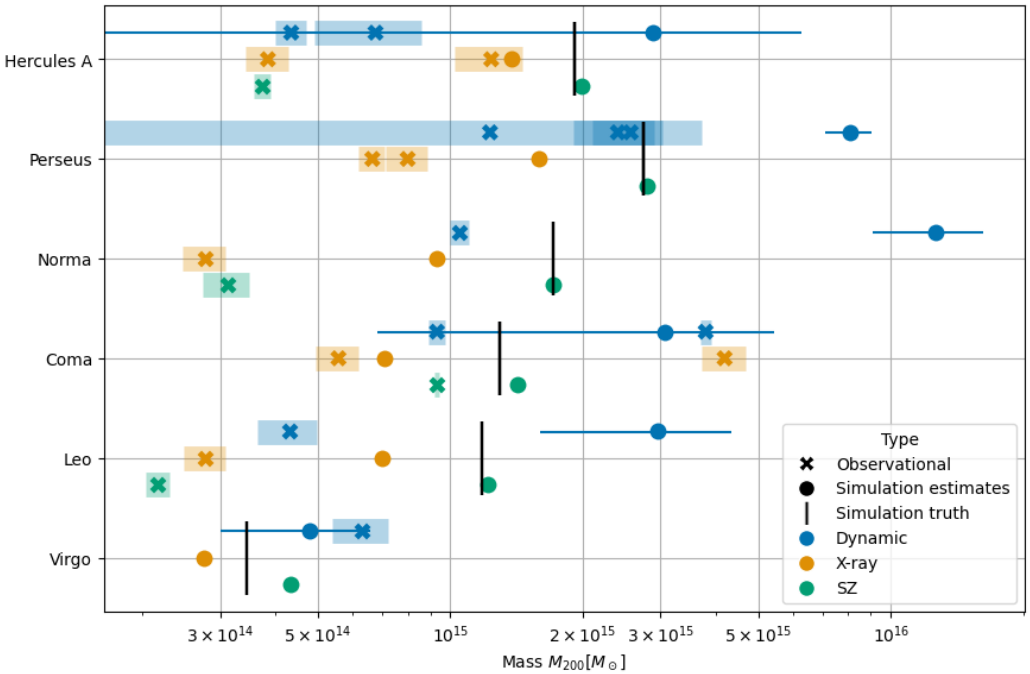

Figure 5.1: Comparison of the six clusters' observational and simulation mass estimates.
All masses are given as M_{200}. In cases where only M_{500} was known, a conversion factor of 1.3 was used. This particular conversion factor was chosen since it was also used by (Stopyra et al., 2021), which makes comparison possible.
For each cluster, the data points are colour-coded based on the method used to achieve the result: The dynamical method points are blue, the X-ray luminosity results are yellow, and results based on the Sunyaev-Zeldovich effect are green. The height in which they are plotted is slightly offset with the dynamical points above the line associated with the cluster name and the SZ points slightly below. The true simulation M_{200} value from the catalogue is indicated as a vertical black line. Thus, this value can be compared to the results from all three methods.
The mass measurement results obtained using a Milky Way perspective presented in the last three chapters are represented by circles in the respective colours. The error bars for them were determined by calculating the standard deviation of all four results of each method (i.e. MW, x, y, and z perspectives). The error bars of the dynamical method are visible. However, the error bars of the other two methods are obscured behind the circle of the data point due to perspective having such a small influence on the results of the X-ray and SZ methods.
The data points marked by an x are observational results from various papers and surveys. Their errors are indicated using a semi-translucent rectangle. These mass estimates and their sources are discussed further in the main text of this chapter.

equation (3.6) from Lovisari et al. (2020) assumes hydrostatic equilibrium.

In addition to comparing the methods, we will compare each simulation estimate to observational mass estimates. These comparisons can be seen in Figure 5.1. The X-ray results with identical error bar widths in the figure are from Piffaretti et al. (2011), the database of which does not include the uncertainty. Therefore, the error bars on those data points are taken from Stopyra et al. (2021).

We then looked at each of the six clusters and their mass estimates from SIBELIUS-FLAMINGO and the various observational estimates seen in Figure 5.1 in detail:

Hercules A All simulation results of the Hercules A cluster are about an order of magnitude larger in the simulation than most of the observational results shown in Figure 5.1, however, one of the X-ray surveys (Babyk and Vavilova, 2013) is in agreement with the simulation X-ray estimate. The region surrounding this cluster included many other objects nearby which is visible in Figure 1.2a. As such a discrepancy between observational and simulation mass results is unsurprising.

The dynamic observational results are taken from Lopes et al. (2018) (the higher estimate) and Kopylova and Kopylov (2013) (the lower estimate). The X-ray results are taken from Babyk and Vavilova (2013) (the higher value) and Piffaretti et al. (2011) (the lower value). The observational Sunyaev-Zeldovich effect result is from Planck Collaboration (2016).

Perseus The dynamical observational result of the Perseus-Pisces cluster is the only observational result whose error bars reach into the catalogue M_{200} value.

The dynamical observational results of the Perseus-Pisces cluster are from Meusinger et al. (2020) (the highest estimate), Escalera et al. (1994) (the middle estimate), and Aguerri et al. (2020) (the lowest estimate). The X-ray results are from Simionescu et al. (2011) (the highest value) and Piffaretti et al. (2011) (the lowest value).

Norma This cluster is a good example of the general trend of the dynamical mass estimate in the simulation being significantly higher than the X-ray and SZ estimates, as well as higher than the simulation truth. The observational values also have a much higher dynamical mass than the X-ray or SZ value, while this dynamical mass is quite close to the simulation X-ray value.

The dynamical, X-ray, and Sunyaev-Zeldovich effect observational mass estimates for the Norma cluster are from Woudt et al. (2008), Piffaretti et al. (2011), and Planck Collaboration (2016), respectively.

Coma The Coma cluster results are in good agreement with each other and the catalogue. On the side of the observations, the X-ray is the furthest from the catalogue, in both the upper and lower limits. On the side of the simulation, it is the dynamic method that is furthest, most likely due to randomly aligned galaxies outside of the cluster contaminating the result.

The dynamical and X-ray results for the Coma cluster are from Babyk and Vavilova (2013) (the highest values) and Rines et al. (2003) (the lowest dynamical value), and Piffaretti et al. (2011) (the lowest X-ray value). The Sunyaev-Zeldovich effect result is from Planck Collaboration (2016).

Leo The observational and simulation results show a similar trend as the values for the Norma cluster. The simulation has significantly higher values than the observations, with the dynamical method in both cases being the highest.

The dynamical, X-ray, and Sunyaev-Zeldovich effect results for the Leo cluster are from Rines et al. (2003), Piffaretti et al. (2011), and Planck Collaboration (2016), respectively.

Virgo Both simulation and observational results lie relatively close to the catalogue value. Since the Virgo cluster is closest to the Milky Way, the Hubble flow rate is significantly lower and thus less noise can be expected for the dynamic method especially. The low mass of Virgo and proximity to the Milky Way makes it challenging for mass estimates to be made based on real X-ray or SZ observations.

The dynamical mass estimate for the Virgo cluster is from Kashibadze et al. (2020).

Another common method of mass measurement is the Weak Lensing. It would be beneficial to include this mass measurement method in future research comparing cluster mass measurement methods. While strong gravitational lenses show multiple images of one background object, weak gravitational lenses distort the images of background galaxies. The distorted images of a few background galaxies are not enough to make conclusions about the mass of the lens, as the viewing angle from the line of sight can also make a galaxy look stretched. Therefore, a statistically

significant number of background galaxies is needed to estimate the mass from the lens. Compared to the methods used in this project, an advantage of the Weak Lensing method is that one measures the cluster mass directly, instead of converting other observables like galaxy velocities or the thermodynamical properties of the cluster's gas.

5.2 Cluster masses in the local environment

The masses of clusters in the cosmic neighbourhood of the Milky Way can be used to test cosmological models and shine a light on open questions in cosmology. These questions include the Hubble (H_0) tension as well as the the σ_8-tension. Therefore, precise measurement of cluster masses is important.

On the one hand, if the clusters generally are less massive than expected from traditional dynamical measurements, the overall average density of the local environment would be lower in effect. In the most extreme case, this could contribute to the Hubble tension as the local expansion rate of a significantly underdense region would be higher than the average expansion rate of the universe. The question of whether or not the Milky Way is part of a large underdense cosmological region is thus essential to verify cosmological models. If this were true for all clusters in our cosmic neighbourhood, this would mean that the total mass in this region was lower than previously assumed. Such an under-density could contribute to the Hubble tension as the cosmic expansion rate locally would be higher than the average rate (Keenan et al., 2013). As long as mass estimates are in disagreement about the matter content in the largest clusters in the region, the overall local density cannot be quantified to a sufficient degree.

On the other hand, a large number of high mass clusters in any given cosmological region would be unlikely given the current constraints from ΛCDM. Generally, ΛCDM constricts the number of very massive clusters in a given region. Stopyra et al. (2021) considered the likelihood of the number of massive clusters in our cosmological neighbourhood. This depends on the choice of σ_8. Generally, the X-ray and especially the SZ mass estimates are lower than the dynamical estimates. The likelihood calculations of Stopyra et al. (2021) favour between no and a few clusters in the local environment having a mass larger than $10^{15}h\mathrm{M}_\odot$. They conclude that ΛCDM would be unlikely if the dynamical mass estimation method were more accurate than SZ and X-ray.

The local clusters in the SIBELIUS-FLAMINGO are very massive. As discussed in McAlpine et al. (2022) within the context of SIBELIUS-DARK

(which has very similar masses to SIBELIUS-FLAMINGO, see Table (1.1)), the simulation masses can be interpreted as a prediction for an abundance of very massive clusters in the local environment. However looking at Figure 5.1, the mass measurement results using SIBELIUS-FLAMINGO compared to observational mass measurements suggest that the true masses in the SIBELIUS simulations are higher than their masses in the physical universe.

We have shown that within SIBELIUS-FLAMINGO, the simulation truth lies closest to the results from the SZ effect method. While these simulation results are significantly higher than real SZ effect observations, this suggests that SZ effect results are more reliable than dynamical mass measurements. Applying that to the real observations considered here, this suggests that the true masses of the observed clusters are closer to the lower SZ estimates. The number of massive clusters in the local environment is therefore most likely within the range expected by ΛCDM based on the abundance predicted by Stopyra et al. (2021). However, these lower masses of the clusters are not sufficient to draw conclusions about the Hubble tension.

5.3 Conclusion

This research aimed to compare the dynamical, X-ray, and SZ effect methods for mass measurement of galaxy clusters. These methods were applied to six clusters (Hercules A, Perseus, Norma, Coma, Leo, and Virgo) in the SIBELIUS-FLAMINGO simulation. The resulting mass measurements of the three methods were compared to the true simulation value and to observational mass measurements of the same clusters.

The Sunyaev-Zeldovich mass in the simulation is by far closest to the true simulation M_{500} as seen above, suggesting that the SZ effect is the most precise of the discussed methods. Generalising this to observational SZ mass estimates, which tend to predict lower masses than most of the dynamical masses and some of the X-ray masses, suggests that there are fewer supermassive clusters in the local cosmic environment than predicted by dynamical mass estimates. This means the abundance of supermassive clusters is not greater than expected within ΛCDM.

The results of this study were primarily qualitative, as it was limited to a small sample size of six clusters. Future research could use the methods outlined in this thesis on a larger simulation with more clusters or multiple simulations to get statistically significant results on how the three methods perform. These results could then be used to improve mass es-

timates based on observations of clusters in the local environment. Additionally, investigating how precisely the Weak Lensing method predicts galaxy cluster masses, could further the precise measurement of cluster masses as it is more directly observable than the results from the three methods used here.

This study underlines the need to refine the methods used in cluster mass measurement. Of the methods investigated in this thesis, the Sunyaev-Zeldovich effect gave the closest results and should be considered to be a reliable method of cluster mass estimation.

Chapter 6

Acknowledgements

I would like to express my deepest gratitude to Matthieu Schaller for his supervision, support, patience, and academic guidance throughout this project. Thanks also go to Joop Schaye and the rest of the simulation group at Leiden Observatory. I would furthermore like to thank the Sibelius group members that I had the joy of discussing this research project with. Thank you to my supportive and diligent proofreaders, Lara and Kristian.

Bibliography

J. A. L. Aguerri, M. Girardi, I. Agulli, A. Negri, C. Dalla Vecchia, and L. Domínguez Palmero. Deep spectroscopy in nearby galaxy clusters - V. The Perseus cluster. MNRAS, 494(2):1681–1692, May 2020. doi: 10.1093/mnras/staa800.

I. V. Babyk and I. B. Vavilova. Comparison of Optical and X-ray Mass Estimates of the Chandra Galaxy Clusters at $z < 0.1$. *Odessa Astronomical Publications*, 26:175, Jan. 2013.

J. Borrow and A. Borrisov. swiftsimio: A python library for reading swift data. *Journal of Open Source Software*, 5(52):2430, 2020. doi: 10.21105/joss.02430. URL https://doi.org/10.21105/joss.02430.

J. Borrow and A. J. Kelly. Projecting sph particles in adaptive environments, 2021.

J. M. Comerford and P. Natarajan. The observed concentration-mass relation for galaxy clusters. *Monthly Notices of the Royal Astronomical Society*, 379(1):190–200, 06 2007. ISSN 0035-8711. doi: 10.1111/j.1365-2966.2007.11934.x. URL https://doi.org/10.1111/j.1365-2966.2007.11934.x.

P. J. Elahi, R. Cañas, R. J. J. Poulton, R. J. Tobar, J. S. Willis, C. d. P. Lagos, C. Power, and A. S. G. Robotham. Hunting for galaxies and halos in simulations with VELOCIraptor. PASA, 36:e021, May 2019. doi: 10.1017/pasa.2019.12.

E. Escalera, A. Biviano, M. Girardi, G. Giuricin, F. Mardirossian, A. Mazure, and M. Mezzetti. Structures in Galaxy Clusters. ApJ, 423:539, Mar. 1994. doi: 10.1086/173833.

J. Jasche and G. Lavaux. Physical Bayesian modelling of the non-linear matter distribution: New insights into the nearby universe. A&A, 625: A64, May 2019. doi: 10.1051/0004-6361/201833710.

O. G. Kashibadze, I. D. Karachentsev, and V. E. Karachentseva. Structure and kinematics of the Virgo cluster of galaxies. A&A, 635:A135, Mar. 2020. doi: 10.1051/0004-6361/201936172.

R. C. Keenan, A. J. Barger, and L. L.Cowie. Evidence for a ∼300 megaparsec scale under-density in the local galaxy distribution. *The Astrophysical Journal*, 775, 2013. URL `https://api.semanticscholar.org/CorpusID:118433293`.

F. G. Kopylova and A. I. Kopylov. Investigation of properties of galaxy clusters in the Hercules supercluster region. *Astronomy Letters*, 39(1): 1–16, Jan. 2013. doi: 10.1134/S1063773712120043.

P. A. A. Lopes, M. Trevisan, T. F. Laganá, F. Durret, A. L. B. Ribeiro, and S. B. Rembold. Optical substructure and BCG offsets of Sunyaev-Zel'dovich and X-ray-selected galaxy clusters. MNRAS, 478(4):5473–5490, Aug. 2018. doi: 10.1093/mnras/sty1374.

L. Lovisari, G. Schellenberger, M. Sereno, S. Ettori, G. W. Pratt, W. R. Forman, C. Jones, F. Andrade-Santos, S. Randall, and R. Kraft. X-Ray Scaling Relations for a Representative Sample of Planck-selected Clusters Observed with XMM-Newton. ApJ, 892(2):102, Apr. 2020. doi: 10.3847/1538-4357/ab7997.

S. McAlpine, J. C. Helly, M. Schaller, T. Sawala, G. Lavaux, J. Jasche, C. S. Frenk, A. Jenkins, J. R. Lucey, and P. H. Johansson. SIBELIUS-DARK: a galaxy catalogue of the local volume from a constrained realization simulation. MNRAS, 512(4):5823–5847, June 2022. doi: 10.1093/mnras/stac295.

H. Meusinger, C. Rudolf, B. Stecklum, M. Hoeft, R. Mauersberger, and D. Apai. The galaxy population within the virial radius of the Perseus cluster. A&A, 640:A30, Aug. 2020. doi: 10.1051/0004-6361/202037574.

H. Mo, F. van den Bosch, and S. White. *Galaxy Formation and Evolution*. Cambridge University Press, 2010.

R. Piffaretti, M. Arnaud, G. W. Pratt, E. Pointecouteau, and J. B. Melin. The MCXC: a meta-catalogue of x-ray detected clusters of galaxies. A&A, 534:A109, Oct. 2011. doi: 10.1051/0004-6361/201015377.

Planck Collaboration. Planck 2013 results. XX. Cosmology from Sunyaev-Zeldovich cluster counts. A&A, 571:A20, Nov. 2014. doi: 10.1051/0004-6361/201321521.

Planck Collaboration. Planck 2015 results. XXVII. The second Planck catalogue of Sunyaev-Zeldovich sources. A&A, 594:A27, Sept. 2016. doi: 10.1051/0004-6361/201525823.

K. Rines, M. J. Geller, M. J. Kurtz, and A. Diaferio. CAIRNS: The Cluster and Infall Region Nearby Survey. I. Redshifts and Mass Profiles. AJ, 126 (5):2152–2170, Nov. 2003. doi: 10.1086/378599.

T. Sawala, S. McAlpine, J. Jasche, G. Lavaux, A. Jenkins, P. H. Johansson, and C. S. Frenk. The SIBELIUS Project: E Pluribus Unum. MNRAS, 509 (1):1432–1446, Jan. 2022. doi: 10.1093/mnras/stab2684.

M. Schaller, C. S. Frenk, R. G. Bower, T. Theuns, J. Trayford, R. A. Crain, M. Furlong, J. Schaye, C. Dalla Vecchia, and I. G. McCarthy. The effect of baryons on the inner density profiles of rich clusters. MNRAS, 452(1): 343–355, Sept. 2015. doi: 10.1093/mnras/stv1341.

M. Schaller et al. Swift: A modern highly-parallel gravity and smoothed particle hydrodynamics solver for astrophysical and cosmological applications. *arXiv e-prints*, art. arXiv:2305.13380, May 2023. doi: 10.48550/arXiv.2305.13380.

J. Schaye, R. Kugel, M. Schaller, J. C. Helly, J. Braspenning, W. Elbers, I. G. McCarthy, M. P. van Daalen, B. Vandenbroucke, C. S. Frenk, J. Kwan, J. Salcido, Y. M. Bahé, J. Borrow, E. Chaikin, O. Hahn, F. Huško, A. Jenkins, C. G. Lacey, and F. S. J. Nobels. The FLAMINGO project: cosmological hydrodynamical simulations for large-scale structure and galaxy cluster surveys. MNRAS, 526(4):4978–5020, Dec. 2023. doi: 10.1093/mnras/stad2419.

A. Simionescu, S. W. Allen, A. Mantz, N. Werner, Y. Takei, R. G. Morris, A. C. Fabian, J. S. Sanders, P. E. J. Nulsen, M. R. George, and G. B. Taylor. Baryons at the Edge of the X-ray-Brightest Galaxy Cluster. *Science*, 331 (6024):1576, Mar. 2011. doi: 10.1126/science.1200331.

S. Stopyra, H. V. Peiris, A. Pontzen, J. Jasche, and P. Natarajan. Quantifying the rarity of the local super-volume. MNRAS, 507(4):5425–5431, Nov. 2021. doi: 10.1093/mnras/stab2456.

P. A. Woudt, R. C. Kraan-Korteweg, J. Lucey, A. P. Fairall, and S. A. W. Moore. The Norma cluster (ACO 3627) - I. A dynamical analysis of the most massive cluster in the Great Attractor. MNRAS, 383(2):445–457, Jan. 2008. doi: 10.1111/j.1365-2966.2007.12571.x.

Y. B. Zeldovich and R. A. Sunyaev. The Interaction of Matter and Radiation in a Hot-Model Universe. Ap&SS, 4(3):301–316, July 1969. doi: 10.1007/BF00661821.